LES eulerian diffuse-interface modeling of fuel dense sprays near- and far-field

J.M. Desantes[a], J.M. García-Oliver[a], J.M. Pastor[a,*], I. Olmeda[a], A. Pandal[b], B. Naud[c]

[a] *CMT-Motores Térmicos, Universitat Politècnica de València, Spain*
[b] *Área de Mecánica de Fluidos - Dpto. Energía, Universidad de Oviedo, Spain*
[c] *Modelling and Numerical Simulation Group, Energy Department,CIEMAT, Spain*

Abstract

Engine fuel spray modeling still remains a challenge, especially in the dense near-nozzle region. This region is difficult to experimentally access and also to model due to the complex and rapid liquid and gas interaction. Modeling approaches based on Lagrangian particle tracking have failed in this area, while Eulerian modeling has proven to be particularly useful. Interface resolved methods are still limited to primary atomization academic configurations due to excessive computational requirements. To overcome those limitations, the single-fluid diffuse interface model known as Σ-Y, arises as a single-framework for spray simulations. Under the assumption of scale separation at high Reynolds and Weber numbers, liquid dispersion is modeled as turbulent mixing of a variable density flow. The concept of surface area density is used for representing liquid structures, regardless of the complexity of the interface.

In this work, a LES based implementation of the Σ-Y model in the Open-

*Corresponding author
Email address: jopasen@mot.upv.es (J.M. Pastor)

FOAM CFD library is applied to simulate the ECN Spray A configuration. Model assessment is performed for both near- and far-field spray development regions using different experimental diagnostics available from ECN database. The CFD model is able to capture near-nozzle fuel mass distribution and, after Σ equation constant calibration, interfacial surface area. Accurate predictions of spray far-field evolution in terms of liquid and vapor tip penetration and local velocity can be simultaneously achieved. Model accuracy is lower when compared to mixture fraction axial evolution, despite radial distribution profiles are well captured.
Keywords: Large Eddy Simulation, Eulerian, Diesel spray, Atomization, Engine Combustion Network (ECN), OpenFOAM®

1. Introduction

Fuel injection and subsequent spray development are critical factors for fuel-air mixture preparation, combustion and pollutants formation in engines. Atomization of the liquid phase occurs at extremely small length scales and high speeds in current injection systems, which complicates both the investigation and modeling of spray flow, especially in the near-nozzle region. The lack of optical accessibility, except by means of special diagnostic techniques [29, 48], hinders the flow characterization and the development of predictive primary atomization models.

At the most detailed level, complex modeling techniques devoted to capturing the liquid-gas interface [22, 34, 58] have been successfully applied to simulate initial spray development, but the computational requirements can make those calculations impractical for spray applications in combustion sys-

tems due to high Reynolds and Weber numbers. The most common spray modeling approaches, based on the representation of the liquid phase using a Lagrangian framework [17], are not well suited to represent this dense region [5], while fully Eulerian approaches have recently shown their potential to simulate near-nozzle physics [68, 5]. Under these conditions, a separation of the large scale flow features from the atomization process occurring at smaller scales can be assumed, as initially proposed by [64, 65]. Then large scale liquid dispersion is modeled as the turbulent mixing of a variable density fluid. In terms of atomization, the surface density concept, which represents the interfacial area per unit of volume, is introduced. The end result is a diffuse-interface treatment in an Eulerian framework, where unresolved interface features are modeled instead of being tracked.

These diffuse-interface Eulerian spray models have two common elements: a model for the transport of liquid and a model for the evolution of the interfacial surface area. The density of interfacial area is typically denoted by Sigma (Σ) while the liquid fraction is denoted by Y. Hence, we refer to the strictly Eulerian model as a Σ-Y approach, in contrast to ELSA (Eulerian-Lagrangian Spray Atomization), which includes a transition to Lagrangian particle tracking [33].

The transport of the liquid employs mass-averaged convection along with turbulent mixing. This model is derived from basic Favre averaging or filtering [13]. Thus, the accuracy of the liquid fraction transport is largely dependent on the accuracy of the two-phase turbulent modeling. Despite the challenges of such modeling, there is at least an extensive theoretical basis to deal with the unclosed terms [13, 1]. However, the model for the

interfacial surface density evolution is somewhat more speculative, with several unclosed terms [14]. Different interface modeling formulations have been applied to sprays as researchers have explored competing ideas of how these terms should be treated [8, 18, 34, 65].

In the present paper, a LES formulation of the Σ-Y model, based on [8], has been implemented to upgrade previous RANS formulations [21, 43]. This approach is assessed for compression ignition (CI) engine injection conditions, corresponding to the Engine Combustion Network (ECN) [20] Spray A. The potential of Σ-Y together with a LES turbulence approach for improved accuracy predictions of spray fuel distribution in the near-nozzle region has been recently shown by the authors [16] and in [2], compared to previous RANS based simulations [15, 44, 68]. Further assessment for both near- and far-field liquid dispersion is performed in the present work.

Far-field analysis requires the consideration of the fuel phase change process when injected at high-temperature and pressure conditions. According to experimental results by Siebers at Sandia National Laboratory (SNL) [59, 60, 61], the vaporization of CI (Diesel) sprays has been described as 'mixing-controlled', that implies faster interfacial mass and energy transport than turbulent mixing. The theoretical analysis performed by Poursadegh et al.[51], based on droplet formation and vaporization time scales, also indicates that Spray A conditions lies in the range where interfacial transport is not the limiting time scale. Different experimental and numerical studies have recently discussed about the sub- or super-critical regime of those fuel injection conditions [12, 10, 38]. According to [11], Spray A nominal condition still remain in the sub-critical regime, but high temperature and pressures

results in very small surface tension forces and extremely high Weber number. Under these conditions, the gas/liquid interface vanishes quickly and phase-change may be evaluated from local thermal equilibrium assumptions [21, 42, 38]. This approach has been followed in the present work in order to simulate vaporizing sprays and to evaluate model performance downstream the primary atomization region.

Experimental data for validation include near-nozzle x-ray based diagnostics conducted at Argonne National Laboratory (ANL) [29, 26] performed at high-pressure but ambient temperature conditions. Considering primary atomization, the interfacial density predictions have rarely been validated, and these validations have been made in the context of downstream drop size [7, 21]. A few prior examples used DNS simulations [34, 8] for model evaluations, and in this paper the validation is performed via USAXS experiments, which directly measures the interfacial surface density. As for far-field validation, experimental characterization at high temperature from different facilities [4] has been used. In particular, diagnostics include local velocity [39] and mixture fraction [47] values measured by means of Particle Image Velocimetry (PIV) and Rayleigh scattering, respectively. Spray tip penetration has also been validated for both near- and far-field configurations.

After this introduction, the modeling approach and experimental results used for validation are discussed. Next, the model setup is presented, followed by the analysis of results, which has been divided into near-field spray dispersion and surface density, and far field spray development. The paper closes with the main conclusions.

2. Modeling approach

The Σ-Y model [65] proposes that, under large Reynolds and Weber numbers operating conditions, it is possible to assume a separation of the large scale flow features, such as liquid mass transport, from the atomization process occurring at smaller scales. The two-phase flow is then modeled as the turbulent mixing of a variable density fluid with a single velocity field, neglecting the effect of surface tension at large scales. This allows the direct simulation of the bulk fluid motion, while unresolved turbulent transport is modeled using standard closures. In this work, the model is formulated in a LES framework with implicit filtering, where filter size is then equal to the grid spacing, for turbulence modeling . Subgrid LES closures are based on the eddy-viscosity hypothesis and calculated by means of the σ-model [41], using a fixed model constant C_σ=1.5.

An indicator function is used to track the dispersion of the liquid phase, taking a value of unity in the liquid phase and zero in the gas phase. The filtered liquid volume fraction is denoted ($\overline{Y}$) and the mass weighted averaged fraction is defined as ($\tilde{Y} = \frac{\overline{\rho Y}}{\bar{\rho}}$). Favre averaging the transport equation for the liquid mass fraction yields Eq. (1)

$$\frac{\partial \bar{\rho}\tilde{Y}}{\partial t} + \frac{\partial \bar{\rho}\tilde{u}_i\tilde{Y}}{\partial x_i} = -\frac{\partial R_{iY}}{\partial x_i} - S_{evap} \tag{1}$$

where the last term accounts for phase change, which will be later discussed. The unclosed turbulent diffusion term, $R_{iY} = \overline{\rho}(\widetilde{u_i Y} - \tilde{u_i}\tilde{Y})$, that appears due to Favre averaging, can be physically related to relative velocity between phases, as described in [65, 13]. This term is modeled using a standard turbulent gradient flux model, which was successfully applied for Diesel-like

spray compared to DNS results [14]:

$$R_{iY} = \overline{\rho}(\widetilde{u_i Y} - \tilde{u_i}\tilde{Y}) = -\frac{\mu_{sgs}}{Sc_t}\frac{\partial \tilde{Y}}{\partial x_i} \tag{2}$$

where μ_{sgs} is the sub-grid turbulent viscosity and Sc_t is the turbulent Schmidt number. Further developments for turbulent liquid flux closure can be found in [1].

Under the assumption that the two phases form an immiscible mixture, the mass-averaged value of the indicator function is related to the density by:

$$\frac{1}{\bar{\rho}} = \frac{\tilde{Y}}{\rho_l} + \frac{1-\tilde{Y}}{\rho_g} \tag{3}$$

An equation of state is then assigned to each phase. The mixture of gas phases obeys an ideal gas law, while for the liquid phase, density is calculated following the Hankinson-Brobst-Thomson (HBT) correlation [53] that accounts for pressure and temperature effects.

In order to account for liquid spray phase change, both an additional transport equation (4) for vapor fuel mass fraction (Y_v) and also a procedure for calculating the sink/source term, S_{evap}, of eq. 1 have been added. The sub-grid scale flux term $\overline{\rho}(\widetilde{u_i Y_v} - \tilde{u_i}\tilde{Y_v})$ in this equation, is solved by means of a gradient closure as in eq. 1.

$$\frac{\partial \bar{\rho}\tilde{Y}_v}{\partial t} + \frac{\partial \bar{\rho}\tilde{u}_i\tilde{Y}_v}{\partial x_i} = \frac{\partial}{\partial x_i}\left(\frac{\mu_{eff}}{Sc}\frac{\partial \tilde{Y}_v}{\partial x_i}\right) + S_{evap} \tag{4}$$

The phase change model is developed in the framework of the diffuse-interface spray approach, following previous authors proposals [21, 45]. The main underlying hypothesis is that local thermodynamic equilibrium is considered within each computational cell, assuming that interfacial transport

is not limiting fuel vaporization. The liquid-vapor coexistence region is then considered under adiabatic saturation condition in order to calculate the equilibrium vapor fuel mass fraction $Y_{v,sat}$. The sink/source term for fuel liquid/vapor transport equations (S_{evap}) is calculated in terms of a rate needed to achieve this $Y_{v,sat}$. This can be written as in eq. 5, where τ_{evap} is a relaxation time set equal to the computational time step, in order to drive the fuel vapor mass fraction Y_v towards the equilibrium $Y_{v,sat}$ at each time step.

$$S_{evap} = \bar{\rho}\frac{Y_{v,sat} - \tilde{Y}_v}{\tau_{evap}} \tag{5}$$

The following transport equation for the bulk mixture enthalpy is solved:

$$\frac{\partial \bar{\rho}\tilde{h}}{\partial t} + \frac{\partial \bar{\rho}\tilde{u}_i\tilde{h}}{\partial x_i} - \frac{\partial}{\partial x_i}\left(\alpha_{eff}\frac{\partial \tilde{h}}{\partial x_i}\right) = \frac{\partial \bar{p}}{\partial t} + \tilde{u}_i\frac{\partial \bar{p}}{\partial x_i} + \tau_{ij}\frac{\partial \tilde{u}_j}{\partial x_i} \tag{6}$$

Here α_{eff} is the effective turbulent thermal diffusivity and $\tau_{ij}\frac{\partial u_j}{\partial x_i}$ the viscous dissipation. And then mixture temperature is obtained from:

$$\tilde{h}\left(T\right) = \tilde{Y}\cdot h_l\left(T\right) + \left(1-\tilde{Y}\right)\cdot h_g\left(T\right) \tag{7}$$

where h_l and h_g denote the enthalpy of the liquid and gas phases respectively. For the the liquid fuel, the Rowlinson-Bondi equation [53], based upon the principle of corresponding states, is applied, while gas enthalpy is directly obtained from the 7-coefficients NASA polynomials.

The solution of the previous equations fully characterizes the large-scale bulk motion of the flow. As a result of the scales separation, atomization is modeled by solving a transport equation for the evolution of the interfacial surface area density Σ, which is defined as the liquid surface present per unit volume at a given time and spatial position. This modeling approach has

started with the equation adopted by Vallet and Borghi [64], in which nearly all the models in the literature are based. The transport equation for Σ reads as shown in Eq. (8), assuming a first-order closure for the interface relative velocity [34] and then obtained from a turbulent diffusive term, where D_Σ is a suitable diffusion coefficient here taken as sub-grid turbulent viscosity μ_{sgs} over turbulent Schmidt number Sc_t.

$$\frac{\partial \bar{\Sigma}}{\partial t} + \frac{\partial u_j \bar{\Sigma}}{\partial x_j} - \frac{\partial}{\partial x_j}\left(D_\Sigma \frac{\partial \bar{\Sigma}}{\partial x_j}\right) = \frac{\bar{\Sigma}}{\tau_\Sigma}\left(1 - \frac{\bar{\Sigma}}{\bar{\Sigma}_{eq}}\right) + S_{\Sigma_{evap}} + S_{\Sigma_{init}} \qquad (8)$$

The first term at the RHS of this equation represents the surface generation and destruction, which is modelled in a restoration to equilibrium form, where $\bar{\Sigma}_{eq}$ is an equilibrium or critical surface density and τ_Σ is the associate time-scale. The surface energy is assumed locally at dynamic equilibrium with the local kinetic energy in order to estimate this equilibrium surface density. The $S_{\Sigma_{init}}$ term is a proper initialization source term, which is necessary due to the fact that all the terms involved in the equation are proportional to the interface surface density (Σ), and then ensures the computation of interface due to the presence of the two phases. Finally, the $S_{\Sigma_{evap}}$ term accounts for vaporization effects on interface surface [33].

Within this LES simulation framework, the surface density should be postulated to describe the subgrid spray characteristics. Chesnel et al.[8] discussed deeply about the different alternatives and concluded with a description where the presence of a minimum interface area is considered plus the subgrid level surface density. Thus, the total evolution of the density of interfacial surface area is given by:

$$\bar{\Sigma} = \bar{\Sigma}_{min} + \bar{\Sigma}' \tag{9}$$

where $\tilde{\Sigma}_{min}$ corresponds to the "minimal" surface density that can be found for a given value of the resolved liquid volume fraction. It is inversely proportional to the filter length scale (Δ_{LES}), which corresponds to grid spacing. The constant α takes the value 2.4 [8].

$$\bar{\Sigma}_{min} = \frac{\alpha}{\Delta_{LES}} \sqrt{\overline{Y}(1-\overline{Y})} \tag{10}$$

To close Eq.(9), a transport equation for the subgrid surface density is defined in the following terms:

$$\frac{\partial \bar{\Sigma}'}{\partial t} + \frac{\partial \tilde{u}_j \bar{\Sigma}'}{\partial x_j} - \frac{\partial}{\partial x_j}\left(D_\Sigma \frac{\partial \bar{\Sigma}'}{\partial x_j}\right) - C_\Sigma \frac{\bar{\Sigma}}{\tau_t}\left(1 - \frac{\bar{\Sigma}}{\bar{\Sigma}_{eq}}\right) = 0 \tag{11}$$

where the coefficient C_Σ is used to relate the relaxation (τ_Σ) and subgrid turbulent (τ_t) time scales:

$$\frac{1}{\tau_\Sigma} = \frac{C_\Sigma}{\tau_t} = C_\Sigma \frac{\epsilon_{sgs}}{k_{sgs}} \tag{12}$$

where k_{sgs} and ϵ_{sgs} are the subgrid turbulent kinetic energy and dissipation, respectively. Finally, $\bar{\Sigma}_{eq}$, already mentioned, is the equilibrium or critical surface density towards which the local surface density is driven. It is again at least equal to the minimum surface density, and it can be described as a function of the critical Weber number (We_{crit}) [18]:

$$\bar{\Sigma}_{eq} = \tilde{\Sigma}_{min} + \bar{\Sigma}'(We_{crit}) = \tilde{\Sigma}_{min} + 4\ \frac{0.5(\rho_l + \rho_g)\overline{Y}(1-\overline{Y})k_{sgs}}{\sigma\ We_{crit}} \tag{13}$$

This LES formulation does not require a initialization term such as in eq. 8 due the presence of a minimum surface density $\tilde{\Sigma}_{min}$ (see eq. 9 and eq. 11). A term accounting for vaporization effect on $\tilde{\Sigma}'$ has not been yet developed, and then has not been considered in this work. Note that the proposed term for eq. 8 in [33] is valid for dispersed droplets but not for the dense zone where, as it was pointed out by [34], is not clear if vaporization decreases or increases the surface density. Nevertheless, the dependence of $\tilde{\Sigma}_{min}$ and $\bar{\Sigma}_{eq}$ on LVF includes vaporization effects in $\bar{\Sigma}$.

The previously described equations have been implemented into a finite volume solver constructed by using the OpenFOAM [67] CFD library. This implementation is based on the segregated pressure-based approach described in [21, 63]. The pressure-equation for this multiphase compressible flow follows the proposal of [56] and [21]. Spatial discretization uses second-order centered schemes, with convective fluxes solved by the Gamma [25] NVD scheme. Time derivative terms are solved by a second-order backward scheme and time step is defined by a maximum CFL of 0.4.

3. Experimental diagnostics

Experimental results available at the ECN [20] have been used to validate the model results. For all cases, the single-hole Spray A nozzle,with a nominal hole diameter of 90 μm, has been used. A detailed internal nozzle geometric characterization [27], presented in Table 1, has been performed for the injectors, where D, L and r denote nozzle orifice outlet diameter, length and inlet radius, respectively. The nozzle convergence is described by the k-factor, as defined in [36]. This smooth entrance and strong convergent angle

Table 1: Nozzle geometric characteristics for ECN Spray-A injectors

Injector Serial#	D[mm]	L/D[-]	r/D[-]	k-factor
210675	0.0894	11.5	0.23	2.7
210677	0.0837	12.3	0.18	3.2
210678	0.0886	11.8	0.21	2.8

indicate that the nozzle is unlikely to cavitate, providing a simplification of the nozzle/spray connection.

Different type of diagnostics have been used, which will be briefly presented. The interested reader can find further information in the corresponding references [28, 26, 39, 47, 4]. Experimental conditions have been matched as closely as possible to the ECN Spray A specification [20], but injection is performed into an inert nitrogen atmosphere (Table 2). Near-nozzle experiments have been performed in an ambient temperature environment, i.e. non-vaporizing conditions, while far-field ones replicate Spray A ambient temperature, so that evaporation process occurs and the liquid phase disappears. In both cases, the same ambient density is used, which is expected to be a governing parameter in the fuel-air mixing process [40].

Table 2: Injection and ambient conditions for Spray A experiment

Fuel	n-Dodecane
Ambient composition	100% N2
Injection pressure [MPa]	150
Ambient temperature [K]	303/900
Ambient density [kg/m^3]	22.8
Fuel injection temperature [K]	343/363

Those operating conditions results in the non-dimensional flow num-

bers presented in Table 3, showing that the spray operates under very high Reynolds (Re) and Weber (We) numbers. The values for injection and ambient conditions variations performed for USAXS diagnostics presented in section 3.1, are also included in this table.

Table 3: Non-dimensional flow numbers for experimental conditions

Case	Re_l	We_l	We_g	ρ_l / ρ_g
Spray A	4.94 x 10^4	1.03 x 10^6	3.28 x 10^4	31.2
P_{inj}=100 MPa	4.03 x 10^4	6.83 x 10^5	2.19 x 10^4	31.2
P_{inj}=50 MPa	2.85 x 10^4	3.42 x 10^5	1.09 x 10^4	31.2
ρ_{amb}=7.6 kg/m^3	4.94 x 10^4	1.03 x 10^6	1.09 x 10^4	93.7

3.1. Near-nozzle diagnostics

Near nozzle diagnostics include experiments carried out within the first milimeters of spray development after injection. Liquid mass dispersion, surface density and spray penetration are obtained by means X-Ray radiography, Ultra-Small-Angle X-ray Scattering (USAXS) and schlieren visualization.

- X-ray radiography[28] experiments provide a path-length-integrated measure of the fuel density along one beam path through the spray due to the attenuation of beam radiation when travelling through the spray. To measure the spatial distribution of the fuel, a two-dimensional raster-scan approach is used, with each point measured from a different set of spray events. To further improve the signal/noise ratio, each data point is an average of 128-256 individual spray events. Time-resolved data from those injections are used to measure the fuel distribution with respect to time, as well as an average during the steady state. Provided data represent the ensemble averaged three-dimensional fuel

density projected onto a plane. The fuel distribution data are thus reported as a Projected Mass Density (PMD), providing valuable information concerning liquid spray dispersion. Nozzle 210675 was used for these experiments.

- Ultra-Small-Angle X-ray Scattering (USAXS) is based on scattering effects[26], and enables the interrogation of the dense region of the spray providing quantitative information about the complex interface without resorting to the assumption that the liquid is in the form of droplets. The scattering intensity as a function of different vectors was measured at axial distances ranging from 1 to 20 mm downstream of the injection nozzle, at the centerline of the spray, from which the differential cross-section can be calculated, and related to the total shape and surface area per volume of fuel droplets, with post-processing performed using the Irena data analysis package[24]. As in X-ray radiography, nozzle 210675 was used in these measurements.

- In addition to the X-ray diagnostics, high-speed Schlieren visualization performed at SNL [20] has been used in order to characterize spray tip penetration. Nozzle 210677 was used for these experiments, and ambient temperature was 440 K, which can still be considered as a non-vaporizing environment.

3.2. Far-field diagnostics

Far field diagnostics consist of measurements spanning distances from the liquid length until the spray tip within an environment at 900 K. They include variables such as local velocity by means of Particle Image Velocimetry (PIV)

and mixture fraction from Rayleigh Scattering Imaging, as well as global metrics such as spray tip penetration and maximum liquid length.

- Local velocity fields for nozzle 210678 have been quantified at IFPEN constant volume vessel by means of Particle Image Velocimetry (PIV)[39]. A high-speed Nd:YAG laser at 532 nm was used as a pulsed laser source, which produced a light sheet intersecting the spray at the symmetry axis. Images were acquired with a Photron SA1 camera. 20 injection events were recorded, from which ensamble statistics are reported.

- Local mixture fraction has been measured for nozzle 210677 at Sandia constant volume vessel by means of Rayleigh Scattering [47]. In this case, a low-speed Nd:YAG laser was used to form light sheet 40 mm wide and 300 μm thick, also intersecting the spray at the symmetry axis. The sheet spanned distances from the nozzle ranging from 17 to 57 mm. On the collection side, an interference filter at the same wavelength as the laser was coupled to the imaging system, a PIXIS1024B camera.

- In terms of spray global metrics, high-speed imaging has been used to resolve the spray tip penetration and maximum liquid length. The first one is measured by means of schlieren visualization for nozzle 210675 [4], while for the second one both Mie-Scattering (nozzle 210677) and Diffuse Backlight Imaging (nozzle 210675) have been used [37, 46].

4. Model set-up

The computational domain comprises a cylindrical spray chamber with 20 mm in length ($\frac{x}{d} > 200$) and 10 mm in diameter ($\frac{r}{d} > 50$) for near-nozzle calculations. An extended domain of 80 mm x 30 mm has been used for including far-field spray development. There are 30 cells across nozzle outlet diameter (Inj. 210675, see Table 1), resulting in minimum grid spacing of $\sim$ 3 μm. The mesh is stretched in axial and radial directions, with maximum cell sizes of around 100 μm located in the outer edge of the domain, away from the spray zone. The grid consists of 6.7 and 12.6 million hexahedral cells for the near-nozzle and full-spray meshes, with the structure shown in Fig. 1. Grid convergence study has been performed using coarser and finer grid resolutions by modifying cell-to-cell expansion ratios, as indicated in Table 4. Concerning LES results quality assessment, previous work [16] showed that the resolved fraction of the turbulent kinetic energy was over 80 % within the spray region even for coarsest grid, which accomplishes the criteria proposed in [50].

Table 4: Characteristics of the different grid resolutions evaluated

Name	Axial expansion ratio	Radial expansion ratio	Number of cells
Grid 1	1.01	1.05	2.6e6
Grid 2	1.005	1.025	6.7e6
Grid 3	1.003	1.015	11.3e6

Injector flow has not directly included in the LES calculations, which requests an extremely high resolution grid to properly resolve the wall-bounded nozzle flow [2]. This would also require the additional complexity of modeling transient injector needle dynamics for accurate mass-flow rate predictions

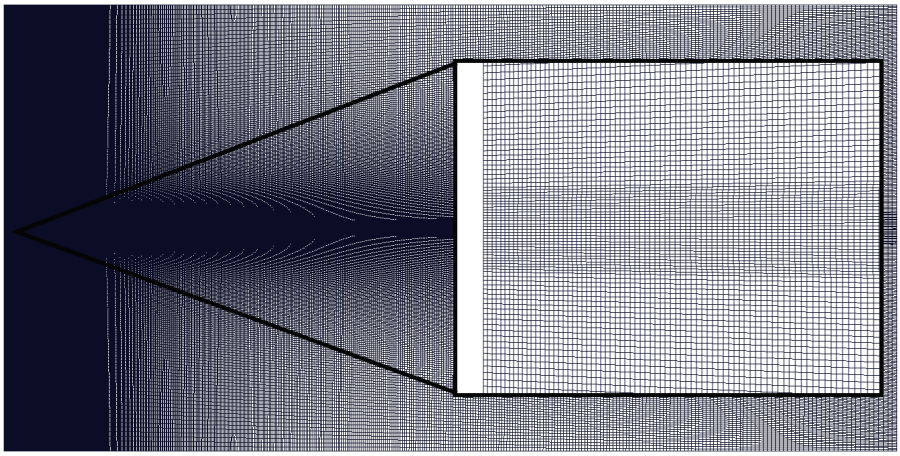

Figure 1: Computational domain slice showing grid structure. The insert shows a zoom around the nozzle outlet.

[3, 6], and then the calculation domain would be limited to the initial spray region for manageable computational costs. Injection conditions are then applied at nozzle outlet by means of an inlet boundary condition (BC) where the time-dependent mass-flow rate [27] obtained from CMT virtual injection rate generator [9], is used in order to get the bulk injection velocity. A synthetic turbulent generator [16], based on the proposals by [31, 30] and following the method described in [55], has been used in order to generate correlated turbulent fluctuations over the mean outlet profile. This profile follows a $1/7^{th}$ power-law and the turbulent intensity (I) was obtained from previous nozzle flow modeling results [44]. As pointed out in [16], this value ranges between 3 and 5 % depending on the turbulence model. A non-slip condition is applied in the surface around the nozzle outlet, while non-reflective BCs

are applied on the other domain surfaces, in order to avoid wave reflection on those open ends. The so-called *waveTransmissive* BC has been used, which is an approximation of the NSCBC [49] that can be applied to the semi-implicit algorithms in OpenFOAM.

5. Results and Discussion

5.1. Near-field spray dispersion

Projected Mass Density (PMD) data has been used in order to evaluate liquid spray dispersion calculations in the near-nozzle region. Line-of-sight integration has been applied to predicted fuel density in order to replicate x-ray radiography measurements. Simulation results are averaged between 0.4 and 1.2 ms after the Start-of-Injection (SoI), such as in experimental data [19]. In Fig. 2 measured and predicted PMD contours are presented, showing that the simulations capture the spray fuel distribution in the near-nozzle region.

A more detailed comparison can be performed from PMD profiles at different axial positions shown in Fig. 3. Experimental data has been centered about the FWHM in order to correct asymmetries due to offset hole on the nozzle tip and spray axis tilt [48]. It is shown that the model is able to accurately predict PMD profiles shortly after the nozzle outlet, at x=0.1 mm ($\frac{x}{d} \approx 1$), and also from dense spray region (x=2 mm) to more dispersed axial positions (x=6 mm). Concerning grid convergence of CFD results, the finest grids are seen to yield nearly the same results, while the coarser one shows higher peak and narrower profiles when moving to downstream locations. Then the intermediate grid resolution has been used in further calculations.

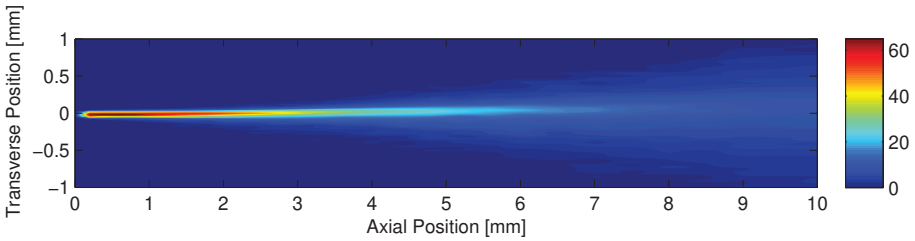

(a) x-ray data

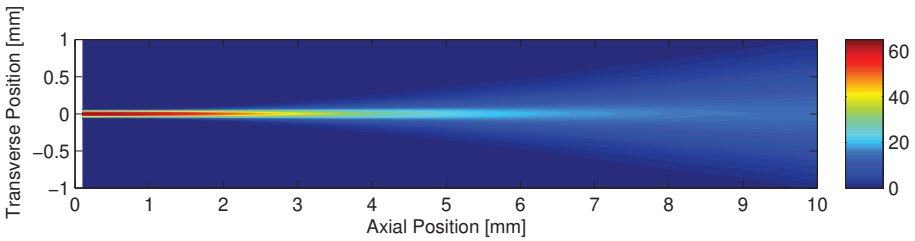

(b) LES I=3% Grid 2 data

Figure 2: Projected mass density $[\mu g/mm^2]$ distributions

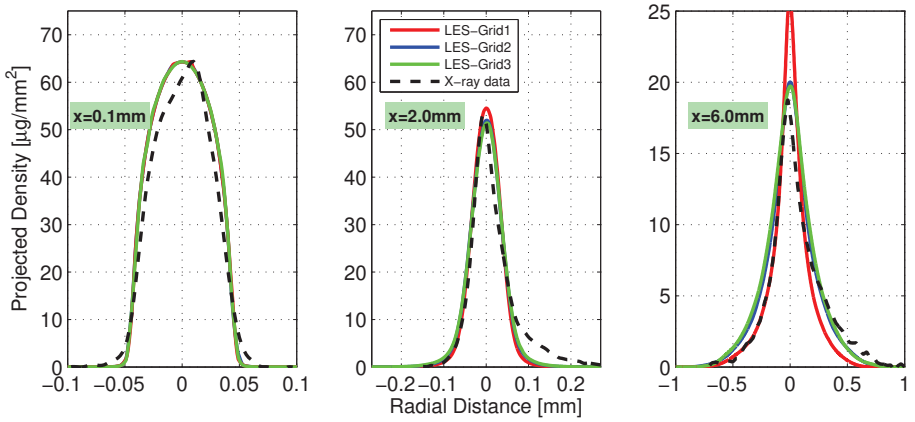

Figure 3: Computed (I=3%) and measured [28] profiles of PMD at axial locations of 0.1 mm, 2 mm, and 6 mm downstream of the nozzle exit

As indicate in Sec. 4, nozzle flow is not included in the calculations, but PMD predictions obtained here are as accurate as recently shown in [2]. They used a similar approach but solving injector flow, which may indicate that

the inlet boundary setup properly reproduces nozzle outlet flow conditions, taking benefit from the simplified geometry of the single-hole tapered high $\frac{L}{D}$ ratio Spray A nozzle. It is then interesting to evaluate the impact of inlet boundary conditions shown Fig. 4: higher turbulence intensities values (I=5%), as used in [32], widens fuel PMD distribution and decrease peak value, showing how initial perturbations affect near-nozzle spray mixing.

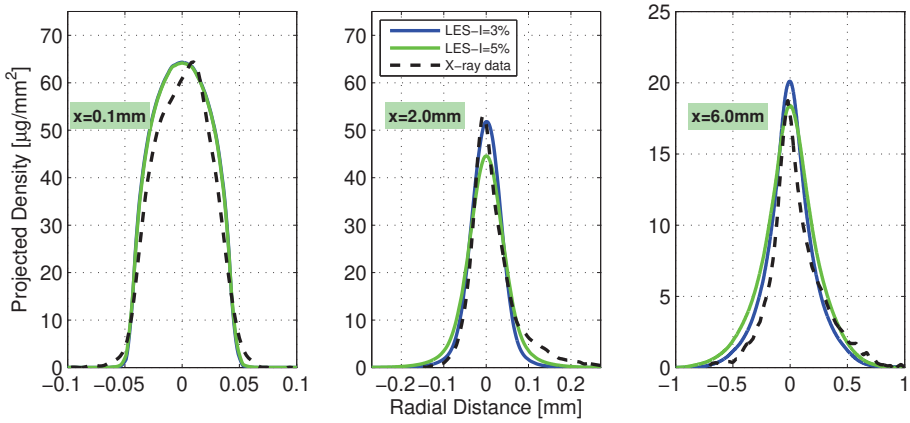

Figure 4: Computed and measured [28] profiles of PMD at axial locations of 0.1 mm, 2 mm, and 6 mm downstream of the nozzle exit

Further insight on spray structure can be obtained from the tomographic reconstruction of the PMD data made by Pickett et al. [48], providing liquid volume fraction (LVF) results. In Fig. 5, the axial profile of the reconstructed LVF is compared with CFD computed profiles, indicating that the model is able to capture the intact core and the LVF profile decay along the spray axis. This result also confirms the model ability to predict fuel spray dispersion from the dense near nozzle to sparse regions downstream. It is also depicted that increasing nozzle outlet turbulent fluctuation from 3 to 5% results in shorter intact core and lower on-axis LVF in the dense spray region.

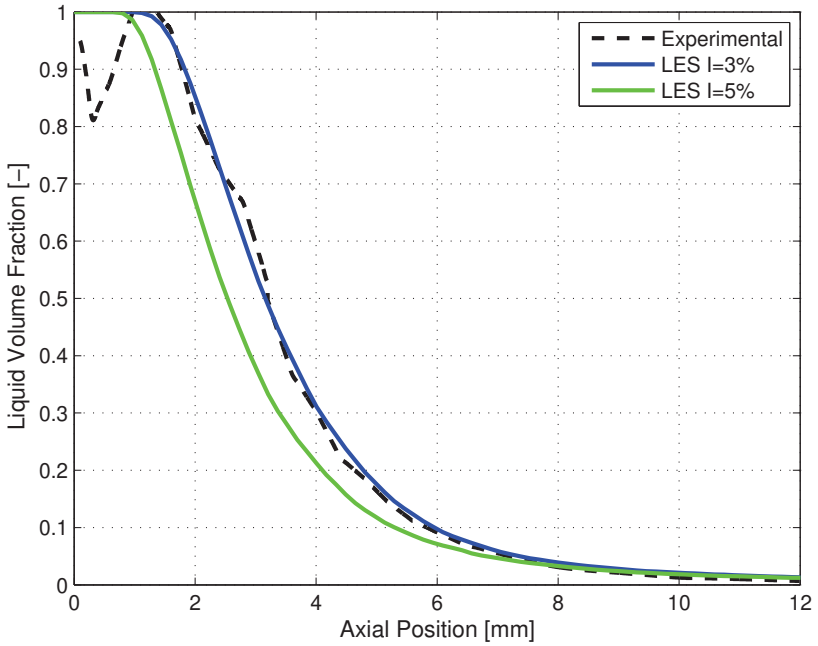

Figure 5: Computed and measured [48] centerline Liquid Volume Fraction

5.2. Spray atomization: surface density

Following the liquid spray dispersion results previously assessed, this section deals with the evaluation of interfacial surface area predictions compared to USAXS results used for spray atomization characterization.

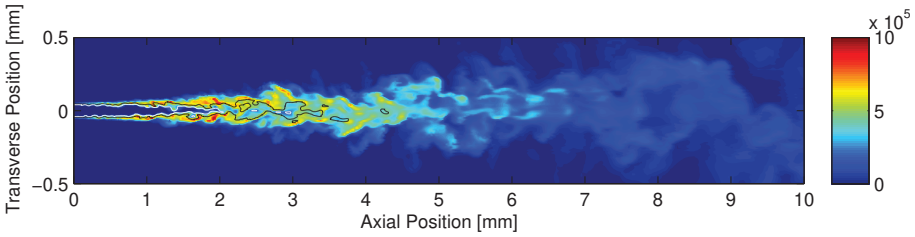

Figure 6: Contours of surface area density ($\bar{\Sigma}$) [m^{-1}] at 1 ms aSOI

As indicated in Sec.2, the equilibrium surface density ($\bar{\Sigma}_{eq}$) defined by a

critical Weber number (We_c), and a relaxation time-scale towards this $\bar{\Sigma}_{eq}$, are required to compute interfacial surface density Σ. Those parameters are yet not fully established, though recent numerical studies based in two-phase DNS results [14, 18] have provided initial insight. In this work, experimental USAXS data [43] have been used to evaluate and select those parameters for further calculations.

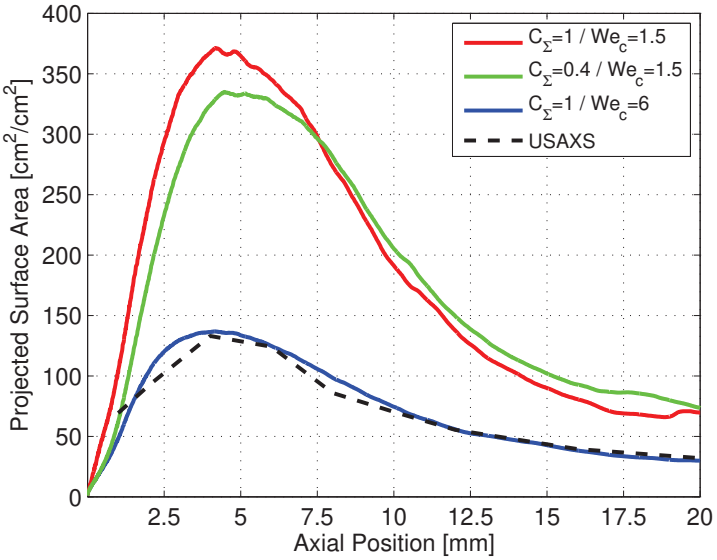

Figure 7: Computed and measured [43] projected surface area on spray axis.

An example of model predictions of Σ at reference condition is presented in Fig. 6. It can be observed that interface production starts after the spray core (defined by LVF=0.9 white iso-line) and peaks downstream, around LVF=0.5 regions indicated by the black iso-line in the figure.

In order to compare with available USAXS data, computational results are time-averaged and projected on the spray axis, which results in path-integrated data presented in Fig. 7. This figure shows the effect of We_c

and C_Σ on the predictions. The proposed $We_c = 1.5$ by [14] results in an over-predicted projected surface area, even with slower relaxation time-scales using $C_\Sigma = 0.4$, as suggested in [18]. Fair agreement was found with We_c=6, which lies in the range proposed by [8].

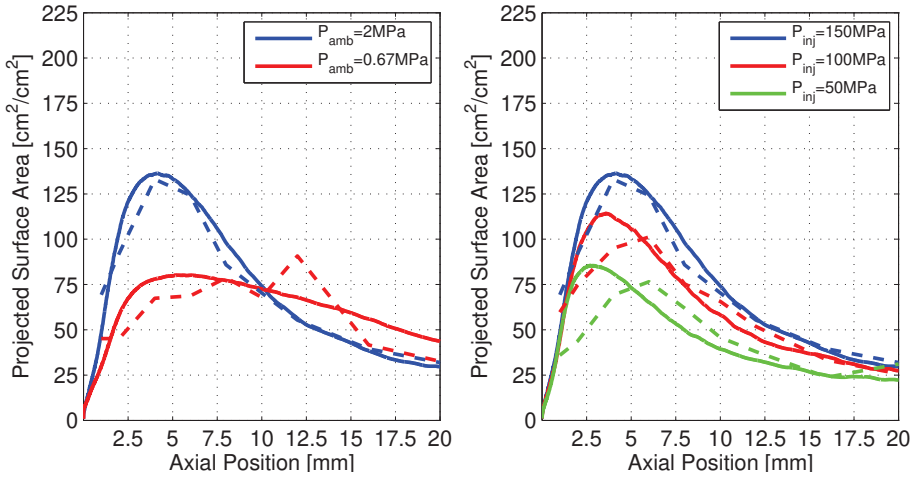

Figure 8: Computed (solid lines) and measured (dotted lines)[43] projected surface area on spray axis. Ambient density (left) and injection pressure (right) variations.

Additional simulations with those constant values for Σ calculation have been performed. Fig. 8 shows that lower ambient density results in a slower interfacial surface growth close to the nozzle, due to slower atomization, which is properly captured by the CFD model. Injection pressure effect is also well predicted by the simulations, i.e. lower injection pressure results in reduced interfacial density (see Fig. 8). In this case the model over-predicts peak projected Σ for reduced injection pressures, despite downstream axial decay is accurately captured. In general, LES predictions improve previous authors results with this modeling approach under a RANS framework [16, 43].

5.3. Far-field spray development: non-vaporizing spray

An important feature of the present modeling approach is the fact that it enables accurate predictions for both near- and far-field spray zones. In the previous section, the analysis has been performed on liquid fuel dispersion and atomization, which happen in the near-field. The present section will show results in the far-field. The analysis starts with the liquid spray tip penetration under non-vaporizing conditions, which actually links both zones. For this purpose Fig. 9 compares modeling and measured results from two independent experimental datasets, namely that from x-ray radiography, which provides detailed information of spray evolution in the initial stages, and schlieren imaging from SNL, which also includes the whole spray evolution, but at the expense of lower spatial and temporal resolutions. Results indicate that the model is able to predict this metric. Extensive studies in the literature (e.g.[40]) have evidenced that Diesel spray tip penetration under both non-vaporizing and vaporizing conditions is governed by momentum exchange between the injected fuel and the ambient gas. In simplified terms, the spray can be considered as a constant momentum flux flow, which entrains air due to the increase in radial width. By simple momentum flux considerations, this exchange between fuel and air results in a decreasing velocity flow, as shown by spray tip evolution. Remarkable accuracy is achieved by the model both during the initial stages as well as later on, when the flow is fully-developed.

Starting with the penetration, Diesel-like fuel sprays injected under engine conditions are known to behave very similarly to a gas jet. This feature has been explored to assess the results of the LES calculations in Fig. 10 and 11.

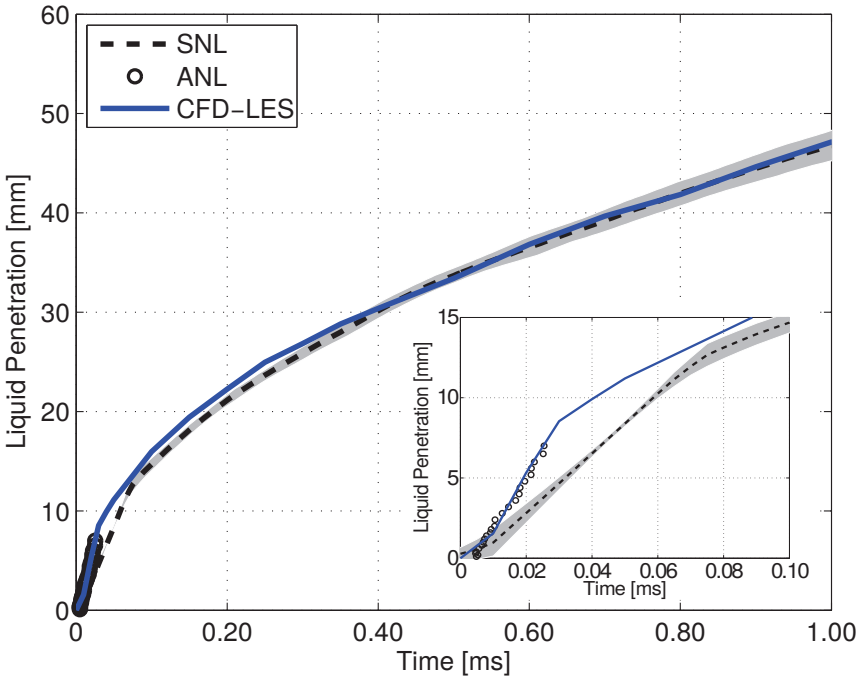

Figure 9: Computed and measured spray tip penetration. The shaded area represents the 95 % confidence interval in measurements. Two datasets are included, the initial penetration from X-ray (Inj. 210675 at T_a=303 K), and the later one from schlieren visualization (Inj. 210677 at T_a=440 K).

First, radial profiles of the normalized mean axial component of the velocity vector (U) are shown at different distances to the nozzle, which evidence a self-similar behaviour, as found in gas jets [23, 62]. This results in a linear increase of the inverse of the axial velocity with the distance to the nozzle, as Fig. 10 shows. A similar behaviour is observed for the fluctuating component of the axial velocity (u'), with self-similar radial distribution, as well as a constant value on the axis with increasing distance to the nozzle (Fig. 11). It must be noted that detailed studies on isodense gas jets, show this self-similarity starting from a distance to the nozzle in the order of 15 and 25

nozzle diameters for the first and second moments [57], respectively . Liquid fuel sprays, however, evolve in a flow with a high density drop. The first consequence is that self-similarity starts from a larger distance to the nozzle, if expressed in terms of nozzle diameters. A more suitable scaling factor is the equivalent diameter $D_{eq} = D\sqrt{\frac{\rho_l}{\rho_g}}$, introduced by Ricou and Spalding [54], which is a more appropriate scaling in cases where fuel-to-ambient density ratio is different from unity. Fig. 10 shows that the self-similar behaviour starts at around 30 D_{eq}, when local to ambient gas density ratio ($\frac{\rho}{\rho_g}$) on the axis levels off.

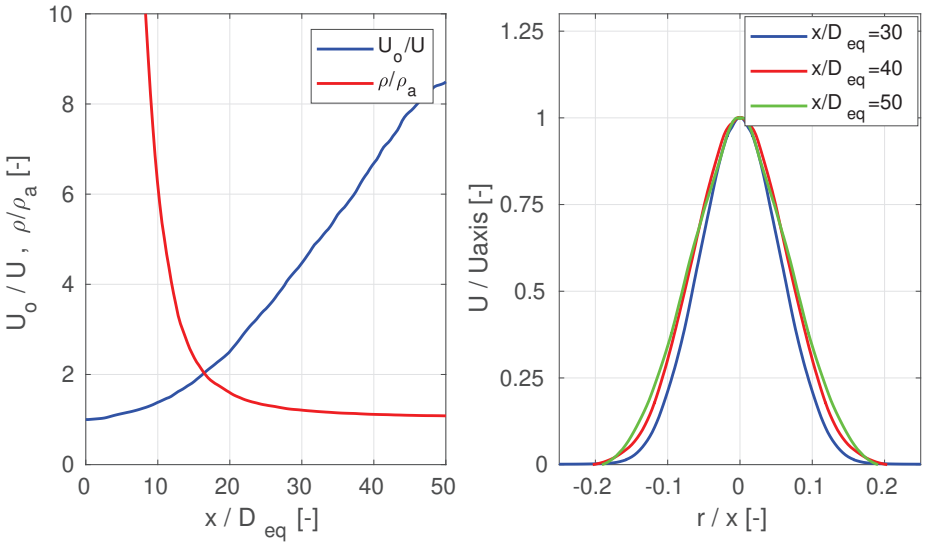

Figure 10: Computed mean normalized axial velocity on the spray axis (left) and at radial cross-sections (right). Left figure also includes the local to ambient density ratio.

5.4. Far-field spray development: vaporizing spray

In addition to the non-vaporizing results presented so far, the model has also been applied for nominal high-temperature ECN Spray A, which corre-

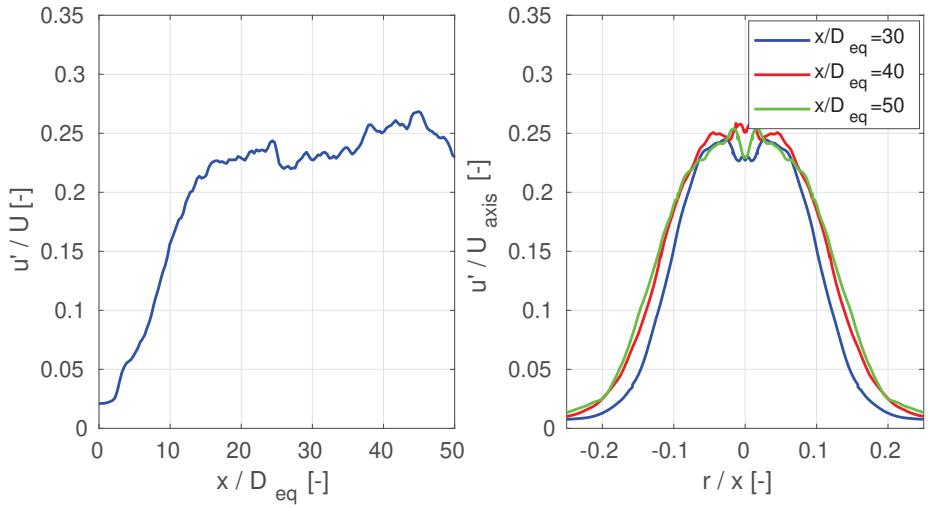

Figure 11: Computed r.m.s fluctuations of axial velocity on the spray axis (left) and at radial cross-sections (right).

sponds to typical CI engine conditions, and multiple experimental diagnostics are available.

Fig. 12 shows simulated vapor and liquid spray penetration, defined according ECN standards [20]. The model fairly agrees with experimental spray evolution for Schlieren imaging [4]. The liquid spray penetration is also well captured by the model, which lies between the experimental data acquired by means of Mie-scattering [4] and DBI [37] techniques. Note that the liquid-length fluctuations are caused by the detached structures in the liquid spray tip shown in Fig. 15. The accuracy of vapor and liquid predictions is similar to that of [38], but the current approach is also able to accurately describe the near-nozzle flow, as previously stated.

This result is backed up by the analysis of local velocity shown in Fig. 13, where both the axial and radial distribution of axial velocity are compared.

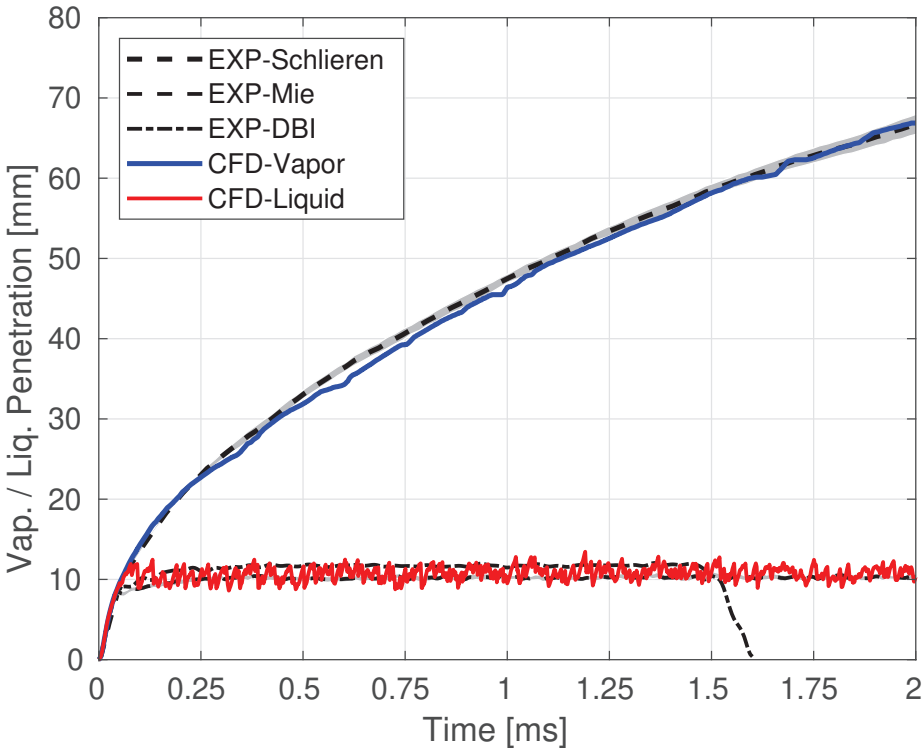

Figure 12: Computed and measured [4] vapor and liquid spray tip penetration. Inj. 210675 and 210677 at nominal Spray A condition T_a=900 K. The shaded area represents the 95 % confidence interval in measurements

Experimental data for comparison [39] are available at 1.5 ms, along the quasi-steady part of the spray. Modelling results have been time-averaged from 1 to 2 ms and radial profiles correspond to azimuthal-averaged data. Accuracy on the axis is remarkable, and radial results have been normalized by those on the axis, showing that the radial width of the flow is also properly predicted, as well as the self-similar features of the axial velocity distribution.

Finally, the model evaluation closes with the comparison of mixture fraction distribution, which corresponds to fuel vapor mass fraction downstream

the liquid spray, in Fig. 14, with a similar layout as in the local velocity case. Averaging of CFD results is performed within the same time window. In this case, the model is seen clearly to underestimate this parameter on the axis, indicating a trend to overmix. In spite of that, radial flow width is properly captured.

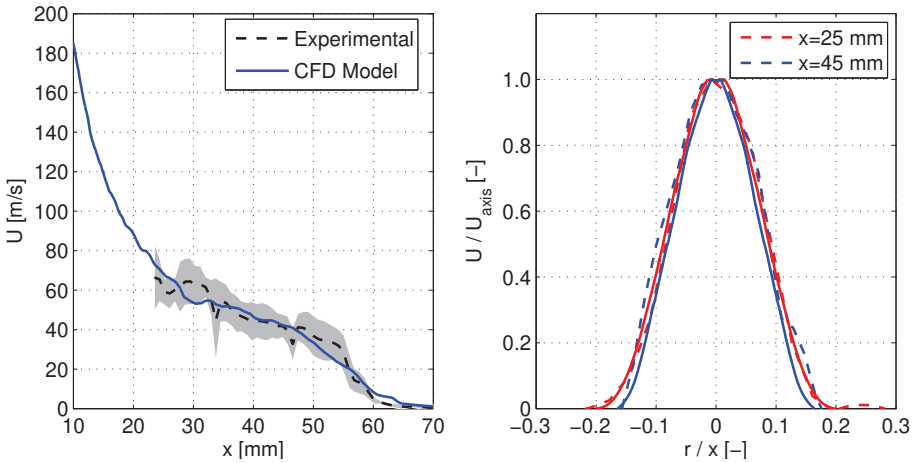

Figure 13: Computed and measured [39] mean axial component of the velocity on the spray axis (left) and at radial cross-sections at x=25 and 45 mm (right). Inj. 210678 at nominal Spray A condition T_a=900 K. The shaded area represents the 95 % confidence interval in measurements.

Until this point, the model has been extensively validated against different experiments, described in section 3, under both non-vaporizing and vaporizing conditions. Note that those diagnostics have provided a detailed description of near-filed spray structure under high-pressure but ambient temperature environment [28, 26], and downstream the liquid spray for vaporizing conditions [39, 47]. Further discussion is provided here on model results that can provide additional insight into the behaviour of the liquid spray under high temperature conditions.

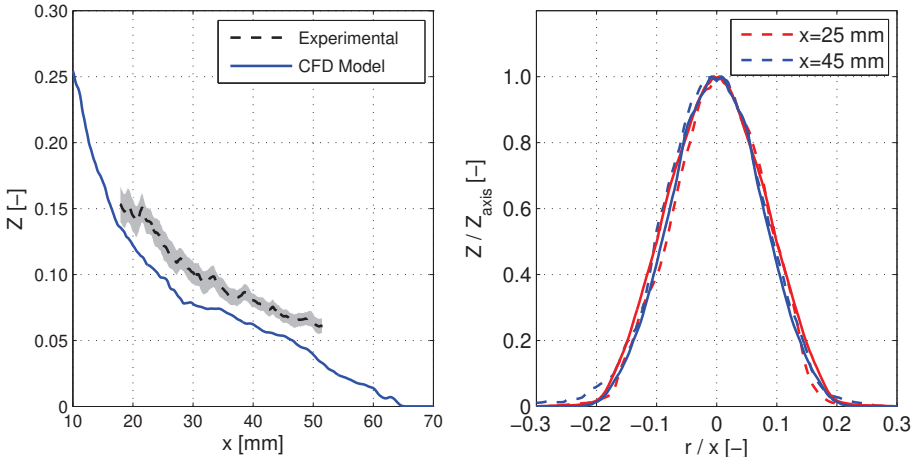

Figure 14: Computed and measured [47] mean mixture fraction (fuel vapor mass fraction) on the spray axis (left) and at radial cross-sections at x=25 and 45 mm (right). Inj. 210677 at nominal Spray A condition T_a=900 K. The shaded area represents the 95 % confidence interval in measurements.

The predicted spray structure is shown at Fig. 15, where the contours of vapor fuel mass fraction and a isosurface of LVF=1.5 x 10^{-3} defining the liquid spray phase limit as suggested in [38], are plotted. Vapor fuel concentration peaks around the liquid spray limit with values close to the saturated vapor-liquid equilibrium fuel mass fraction [45] evaluated from adiabatic mixing and the ambient and fuel boundary conditions.

Fig.16a presents the predicted liquid volume fraction (LVF) contours, where LVF is found to be larger than 0.1 over 50% of the liquid spray length (in the order of 10 mm). This indicates that vaporization takes place within the dense spray region, confirming that local flow is far from being dispersed in terms of droplets. The model also provides the characteristic size of liquid structures in terms of Sauter Mean Diameter (SMD) from Σ and Y predictions ($SMD = \frac{6\bar{Y}}{\bar{\Sigma}}$), an example of which is shown in Fig.16b. The SMD

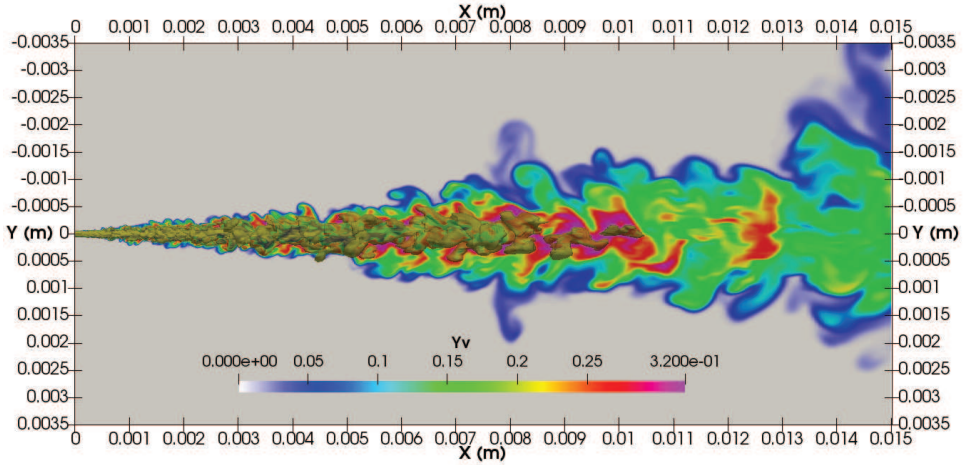

Figure 15: Computed vapor mass fraction (Y_v) on a symmetry plane and LVF=1.5 x 10^{-3} isosurface at nominal Spray A condition T_a=900 K.

abruptly decreases shortly downstream the liquid intact core, in agreement to experimental results combining PMD and USAXS diagnostics [26] performed under non-vaporizing conditions. Further downstream, SMD remains almost stable, with drop sizes around 1-2 x 10^{-6} m in the dense spray regions, also similar to [26] results, and eventually decreases due to vaporization effects as liquid fuel approaches the liquid spray limits.

The characteristic time scales can be obtained from simulation flow conditions in order to evaluate the vaporization modeling approach assumptions. The droplet vaporization time scale, computed as an isolated droplet in a convective environment as [51], from those drop sizes and the relative velocity based on single velocity field fluctuations [52], is $\approx$ 5 x 10^{-7}s. If we estimate the liquid spray mixing time scale from local velocity and vaporization length, it turn out to be $\approx$ 2 x 10^{-5}s, which is also higher than vaporization ones. Even subgrid turbulent time scales are bigger, as shown in Fig.16c,

which indicate values in the order of 2 x 10^{-6} s within the liquid spray.

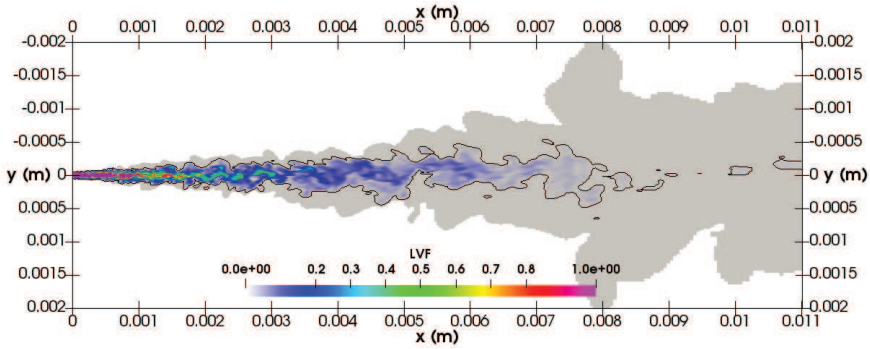

(a) Liquid Volume Fraction (LVF) contours

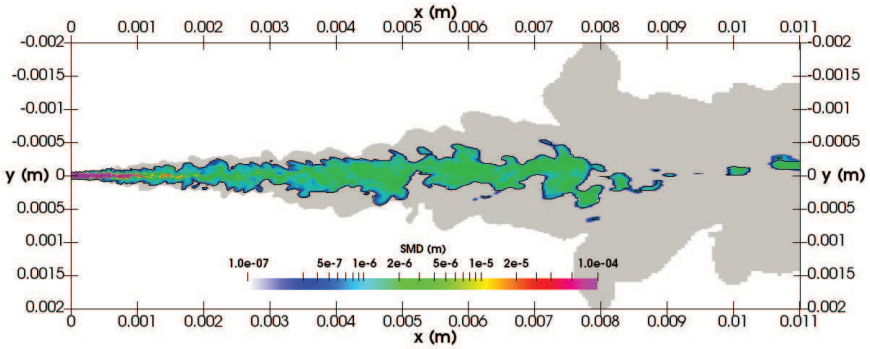

(b) Sauter Mead Diameter (SMD) contours

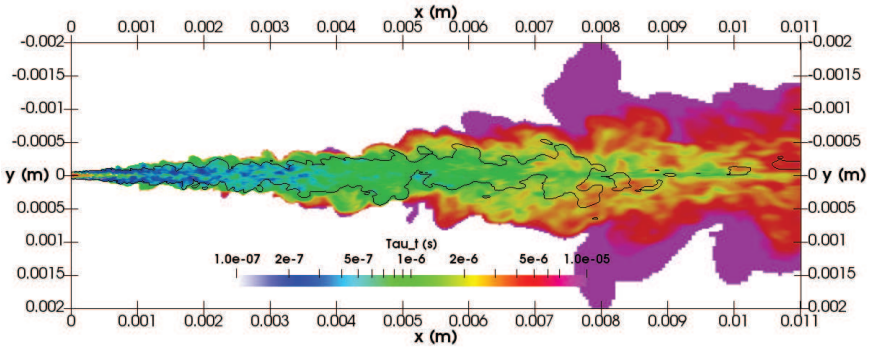

(c) Subgrid turbulent time-scale (τ_t) contours

Figure 16: Computed results on a symmetry plane at nominal Spray A condition T_a=900 K. The shaded contour represents vapor fuel spray defined by Y_v=1 x $10^{-3}$and the black isoline (LVF=1.5 x 10^{-3}) defines the liquid spray.

Summarizing, model results confirm that most of the liquid mass evolves in a high-density region, which is governed by air entrainment. A relatively constant droplet size is obtained from the end of the intact core up to the maximum liquid length, where droplets disappear due to evaporation. The fact that for this type of sprays such processes occur relatively close to the nozzle suggests that particle methods based on dispersed flow assumptions may be not valid for these conditions, and supports the current Eulerian approach based on dynamic and thermal equilibrium.

6. Summary and Conclusions

This work presents a LES implementation of the diffuse-interface Σ-Y spray model applied for high-pressure fuel injection. The model performance has been assessed for complete spray development simulations corresponding to the ECN Spray-A condition.

Near-nozzle spray model validation has been performed by comparing with x-ray radiography data in terms of projected mass density and liquid-volume fraction. Spray flow has been modeled by using a synthetic turbulence boundary condition at the nozzle exit, which replaces expensive nozzle-flow calculations. Fuel dispersion is properly predicted, with accuracy level similar to recent results that include nozzle internal geometry. Nevertheless, it is shown that turbulent fluctuations have a noticeable impact in near-nozzle spray dispersion. Detailed internal flow calculations are then required for a fully predictive calculation of spray development when using more complex nozzle geometries.

Concerning spray atomization, a LES specific formulation has been used for interfacial surface density modeling. Predictions have been directly com-

pared to measurements obtained using USAXS technique. The equilibrium surface density, defined by a critical We number, has been calibrated in a single operation point. Without further adjustment the model was able to predict both injection pressure and ambient density variations, improving previous results. This outcome shows the potential of the LES Σ equation for predicting complex atomization features in those high We and Re dense spray region. It also enables the use of this information for including more complex liquid/gas interaction in fuel dispersion Y-equation.

Besides near-nozzle predictions, far-field spray development has also been evaluated. Global metrics such as spray tip penetration and maximum liquid length are accurately predicted, both under non-vaporizing and vaporizing conditions. Local analysis shows that velocity field predictions also match experimental measurements, so local flow dynamics is well-captured. However, mixture fraction tends to be underpredicted, in spite of the fact that the width of the radial distribution is adequately captured. Similar conclusions can be drawn from other LES calculations of Spray A test case [69, 66], only few approaches [38, 35] are able to capture the mixing field. Nevertheless, none of these cases evaluates at the same time the near-nozzle atomization and spray dispersion together with the far-field spray evolution.

Model results confirm that under ECN Spray A conditions liquid vaporizes within a high density region, where droplet diffusion timescales are much lower than turbulent mixing timescales. These results hint at the limitations in disperse droplet methods, and confirms the advantages of the present modelling approach to capture the evolution of such high dense multiphase flows.

In summary, the present contribution shows that the proposed LES diffuse-interface Eulerian framework can capture both near-nozzle atomization and dispersion features, together with far-field local flow and mixing, with no need for an exhaustive calibration of model constants. This is a highly relevant result for detailed spray calculations with a single framework.

Acknowledgements

This work was partially funded by the Spanish Ministerio de Economía y Competitividad within the frame of the CHEST (TRA2017-89139-C2-1-R) project. The computations were partially performed on the Tirant III cluster of the Servei d'Informàtica of the University of Valencia (vlc38-FI-2018-2-0006). Authors acknowledge the computer resources at Picasso and the technical support provided by Universidad de Málaga (UMA) (RES-FI-2018-1-0039).

Authors also thank the shared X-ray radiography and Ultra-Small-Angle X-ray Scattering measurements performed at Argonne National Laboratory by the following authors: Daniel J. Duke, Jan Ilavsky, Katarzyna E. Matusik, Brandon A. Sforzo, Alan L. Kastengren, and Christopher F. Powell.

References

[1] Andreini, A., Bianchini, C., Puggelli, S., and Demoulin, F. X., Development of a turbulent liquid flux model for Eulerian-Eulerian multiphase flow simulations, *International Journal of Multiphase Flow*, vol. **81**, pp. 88–103, 2016. URL `http://dx.doi.org/10.1016/j.ijmultiphaseflow.2016.02.003`

[2] Anez, J., Ahmed, A., Hecht, N., Duret, B., Reveillon, J., and Demoulin, F., Eulerian-Lagrangian Spray Atomization model coupled with Interface Capturing Method for Diesel injectors, *International Journal of Multiphase Flow*, vol. **113**, pp. 325–342, 2019.
URL `https://www.sciencedirect.com/science/article/pii/S0301932218303550`

[3] Baldwin, E. T., Grover, R. O., Parrish, S. E., Duke, D. J., Matusik, K. E., Powell, C. F., Kastengren, A. L., and Schmidt, D. P., String flash-boiling in gasoline direct injection simulations with transient needle motion, *International Journal of Multiphase Flow*, vol. **87**, pp. 90–101, 2016.
URL `http://dx.doi.org/10.1016/j.ijmultiphaseflow.2016.09.004`

[4] Bardi, M., Payri, R., Malbec, L., Brunneaux, G., Pickett, L., Manin, J., Bazyn, T., and Genzale, C., Engine combustion network: Comparison of spray development,vaporization and combustion in different combustion vessels, *Atomization and Sprays*, vol. **22**, pp. 807–842, 2012.

[5] Battistoni, M., Magnotti, G. M., Genzale, C. L., Arienti, M., Matusik, K. E., Duke, D. J., Giraldo, J., Ilavsky, J., Kastengren, A. L., Powell, C. F., and Marti-Aldaravi, P., Experimental and Computational Investigation of Subcritical Near-Nozzle Spray Structure and Primary Atomization in the Engine Combustion Network Spray D, *SAE Technical Paper*, no. 2018-01-0277, pp. 1–15, 2018.

[6] Battistoni, M., Som, S., and Powell, C. F., Highly resolved Eulerian simulations of fuel spray transients in single and multi-hole injectors: Nozzle flow and near-exit dynamics, *Fuel*, vol. **251**, pp. 709–729, 2019.
URL `https://www.sciencedirect.com/science/article/pii/S0016236119306313`

[7] Beheshti, N., Burluka, A., and Fairweather, M., Assessment of $\Sigma - Y$liq model predictions for air-assisted atomisation, *Theoretical and Computational Fluid Dynamics*, vol. **21**, no. 5, pp. 381–397, 2007.

[8] Chesnel, J., Reveillon, J., Ménard, T., and Demoulin, F. X., Large eddy simulation of liquid jet atomization, *Atomization and Sprays*, vol. **21**, no. 9, pp. 711–736, 2011.

[9] CMT, Virtual injection rate generator, 2018.
URL `http://www.cmt.upv.es`

[10] Crua, C., Heikal, M. R., and Gold, M. R., Microscopic imaging of the initial stage of diesel spray formation, *Fuel*, vol. **157**, pp. 140–150, 2015.
URL `http://dx.doi.org/10.1016/j.fuel.2015.04.041`

[11] Crua, C., Manin, J., and Pickett, L. M., On the transcritical mixing of fuels at diesel engine conditions, *Fuel*, vol. **208**, pp. 535–548, 2017.
URL `http://dx.doi.org/10.1016/j.fuel.2017.06.091`

[12] Dahms, R. N., Manin, J., Pickett, L. M., and Oefelein, J. C., Understanding high-pressure gas-liquid interface phenomena in diesel engines, *Proceedings of the Combustion Institute*, vol. **34**, no. 1, pp. 1667 – 1675, 2013.

[13] Demoulin, F., Beau, P., Blokkeel, G., Mura, A., and Borghi, R., A new model for turbulent flows with large density fluctuations: application to liquid atomization, *Atomization and Sprays*, vol. **17**, pp. 315–345, 2007.

[14] Demoulin, F.-X., Reveillon, J., Duret, B., Bouali, Z., Desjonqueres, P., and Menard, T., Toward using direct numerical simulation to improve primary break-up modeling, *Atomization and Sprays*, vol. **23**, no. 11, pp. 957–980, 2013.

[15] Desantes, J., García-Oliver, J., Pastor, J., Pandal, A., Baldwin, E., and Schmidt, D., Coupled / decoupled spray simulation comparison of the ECN spray a condition with the $\Sigma - Y$ eulerian atomization model, *International Journal of Multiphase Flow*, vol. **80**, pp. 89 – 99, 2016.

[16] Desantes, J. M., García-Oliver, J. M., Pastor, J. M., Pandal, A., Naud, B., Matusik, K., Duke, D., Kastengren, A., Powell, C., and Schmidt, D. P., Modelling and validation of near-field Diesel spray CFD simulations based on the Σ-Y model, *ILASS2017 - 28th European Conference on Liquid Atomization and Spray Systems, September 6-8, Valencia, Spain*, 2017.
URL `http://dx.doi.org/10.4995/ILASS2017.2017.4715`

[17] Dukowicz, J., A particle fluid numerical model for liquid sprays, *Journal of Computational Physics*, vol. **35**, no. 2, pp. 229–253, 1980.

[18] Duret, B., Reveillon, J., Menard, T., and Demoulin, F., Improving primary atomization modeling through dns of two-phase flows, *International Journal of Multiphase Flow*, vol. **55**, pp. 130 – 137, 2013.
URL `http://www.sciencedirect.com/science/article/pii/S0301932213000773`

[19] ECN, LVF data archive, 2014.
URL `http://www.sandia.gov/ecn/argonne/assets/datafiles/mixture/rad675.php`

[20] ECN, Engine combustion network data archive, 2018.
URL `http://www.sandia.gov/ecn/`

[21] García-Oliver, J., Pastor, J., Pandal, A., Trask, N., Baldwin, E., and Schmidt, D., Diesel spray CFD simulations based on the $\Sigma - Y$ eulerian atomization model, *Atomization and Sprays*, vol. **23**, pp. 71–95, 2013.

[22] Gorokhovski, M. and Herrmann, M., Modeling primary atomization, *Annual Review of Fluid Mechanics*, vol. **40**, pp. 343–366, 2008.

[23] Hussein, H. J., Capp, S. P., and George, W. K., Velocity measurements in a high-reynolds-number, momentum-conserving, axisymmetric, turbulent jet, *Journal of Fluid Mechanics*, vol. **258**, p. 31–75, 1994.

[24] Ilavsky, J. and Jemian, P. R., *Irena*: tool suite for modeling and analysis of small-angle scattering, *Journal of Applied Crystallography*, vol. **42**, no. 2, pp. 347–353, 2009.

[25] Jasak, H., Weller, H. G., and Gosman, A. D., High resolution NVD differencing scheme for arbitrarily unstructured meshes, *International Journal for Numerical Methods in Fluids*, vol. **31**, no. 2, pp. 431–449, 1999.

[26] Kastengren, A., Ilavsky, J., Viera, J. P., Payri, R., Duke, D. J., Swantek, A., Tilocco, F. Z., Sovis, N., and Powell, C. F., Measurements of droplet size in shear-driven atomization using ultra-small angle x-ray scattering, *International Journal of Multiphase Flow*, vol. **92**, pp. 131–139, 2017.

[27] Kastengren, A., Tilocco, F. Z., Powell, C. F., Manin, J., Pickett, L. M., Payri, R., and Bazyn, T., Engine combustion network (ECN):measurements of nozzle geometry and hydraulic behavior, *Atomization and Sprays*, vol. **22**, pp. 1011–1052, 2012.

[28] Kastengren, A. L., , Tilocco, F. Z., Duke, D. J., Powell, C. F., Seoksu, M., and Xusheng, Z., Time-resolved x-ray radiography of diesel injectors from the engine combustion network, *ICLASS Paper*, no. 1369, 2012.

[29] Kastengren, A. L., Powell, C. F., Wang, Y., Im, K.-S., and Wang, J., X-ray radiography measurements of diesel spray structure at engine-like ambient density, *Atomization and Sprays*, vol. **19**, no. 11, pp. 1031–1044, 2009.

[30] Klein, M., Sadiki, A., and Janicka, J., A digital filter based generation of inflow data for spatially developing direct numerical or large eddy simulations, *Journal of Computational Physics*, vol. **186**, no. 2, pp. 652–665, 2003.

[31] Kraichnan, R. H., Diffusion by a Random Velocity Field, *Physics of Fluids*, vol. **13**, no. 1, pp. 22 – 30, 1970.
URL `https://aip.scitation.org/doi/10.1063/1.1692799`

[32] Lacaze, G., Misdariis, A., Ruiz, A., and Oefelein, J. C., Analysis of high-pressure diesel fuel injection processes using les with real-fluid thermodynamics and transport, *Proceedings of the Combustion Institute*, vol. **35**, no. 2, pp. 1603 – 1611, 2015.
URL http://www.sciencedirect.com/science/article/pii/S1540748914002302

[33] Lebas, R., Beau, P.-a., Blokkeel, G., and Demoulin, F.-X., ELSA Model for Atomization: To Benefit of the Eulerian and Lagrangian Descriptions of the Liquid Phase, *Proceedings of the 10th International Conference on Liquid Atomization and Spray Systems, ICLASS 2006, Aug.27-Sept.1, Kyoto, Japan*, pp. 565–572, 2006.

[34] Lebas, R., Menard, T., Beau, P., Berlemont, A., and Demoulin, F., Numerical simulation of primary break-up and atomization: DNS and modeling study, *International Journal of Multiphase Flow*, vol. **35**, pp. 247–260, 2009.

[35] Ma, P. C., Wu, H., Jaravel, T., Bravo, L., and Ihme, M., Large-eddy simulations of transcritical injection and auto-ignition using diffuse-interface method and finite-rate chemistry, *Proceedings of the Combustion Institute*, vol. **37**, no. 3, pp. 3303–3310, 2018.
URL https://www.sciencedirect.com/science/article/pii/S1540748918300646

[36] Macián, V., Bermúdez, V., Payri, R., and Gimeno, J., New technique for determination of internal geometry of a diesel nozzles with the use of silicone methodology, *Experimental Techniques*, vol. **37**, pp. 39–43, 2003.

[37] Manin, J., Bardi, M., and Pickett, L. M., Evaluation of the liquid length via diffused back-illumination imaging in vaporizing diesel sprays, *The Proceedings of the International symposium on diagnostics and modeling of combustion in internal combustion engines COMODIA*, vol. **2012.8**, pp. 665–673, 2012.

[38] Matheis, J. and Hickel, S., Multi-component vapor-liquid equilibrium model for LES of high-pressure fuel injection and application to ECN Spray A, *International Journal of Multiphase Flow*, vol. **99**, pp. 294–311, 2018.
URL http://www.sciencedirect.com/science/article/pii/S0301932217301076

[39] Meijer, M., Malbec, L., Brunneaux, G., and Somers, L., Engine combustion network : 'spray a' basic measurements and advanced diagnostics, *Proceedings of the 12th International Conference on Liquid Atomization and Spray Systems, ICLASS 2012, 2-6 September, Heidelberg, Germany*, 2012.

[40] Naber, J. and Siebers, D., Effects of gas density and vaporization on penetration and dispersion of diesel sprays, *SAE Technical Paper*, no. 960034, 1996.

[41] Nicoud, F., Toda, H. B., Cabrit, O., Bose, S., and Lee, J., Using singular values to build a subgrid-scale model for large eddy simulations, *Physics of Fluids*, no. 8, 2011.

[42] Oefelein, J., Dahms, R., and Lacaze, G., Detailed modeling and simulation of high-pressure fuel injection processes in diesel engines, *SAE Int. J. Engines*, vol. **5**, no. 3, pp. 1410 – 1419, 2012.

[43] Pandal, A., Pastor, J. M., Payri, R., Kastengren, A., Duke, D., Matusik, K., Giraldo, J. S., Powell, C., and Schmidt, D., Computational and experimental investigation of interfacial area in near-field diesel spray simulation, *SAE Int. J. Fuels Lubr.*, vol. **10**, pp. 423 – 431, 2017.

[44] Pandal, A., Payri, R., García-Oliver, J., and Pastor, J., Optimization of spray break-up cfd simulations by combining σ-y eulerian atomization model with a response surface methodology under diesel engine-like conditions (ECN Spray A), *Computers and Fluids*, vol. **156**, pp. 9 – 20, 2017.

[45] Pastor, J., García-Oliver, J., Pastor, J., and Vera-Tudela, W., One-dimensional diesel spray modeling of multicomponent fuels, *Atomization and Sprays*, vol. **25**, no. 6, pp. 485–517, 2015.

[46] Pickett, L., Genzale, C., Manin, J., Malbec, L., and Hermant, L., Measurement uncertainty of liquid penetration in evaporating diesel sprays, *ILASS-Americas 2011, Ventura, California, May 15-18, Paper No. 2011-111*, 2011.

[47] Pickett, L., Manin, J., Genzale, C., Siebers, D., Musculus, M., and Idicheria, C., Relationship between diesel fues spray vapor penetration/dispersion and local fuel mixture fraction, *SAE Int. J. Engines*, vol. **4**, pp. 764–799, 2011.

[48] Pickett, L., Manin, J., Kastengren, A., and Powell, C., Comparison of near-field structure and growth of a diesel spray using light-based optical microscopy and x-ray radiography, *SAE Int. J. Engines*, vol. **7**, no. 2, pp. 1044–1053, 2014.

[49] Poinsot, T. and Lelef, S., Boundary conditions for direct simulations of compressible viscous flows, *Journal of Computational Physics*, vol. **101**, no. 1, pp. 104 – 129, 1992.
URL `http://www.sciencedirect.com/science/article/pii/0021999192900462`

[50] Pope, S. B., Ten questions concerning the large-eddy simulation of turbulent flows, *New Journal of Physics*, vol. **6**, 2004.

[51] Poursadegh, F., Lacey, J. S., Brear, M. J., and Gordon, R. L., On the Fuel Spray Transition to Dense Fluid Mixing at Reciprocating Engine Conditions, *Energy and Fuels*, vol. **31**, no. 6, pp. 6445–6454, 2017.

[52] Puggelli, S., Palanti, L., Andreini, A., and Demoulin, F.-X., Development of an evaporation model for the dense spray region in Eulerian-Eulerian multiphase flow simulations, *ILASS2017 - 28th European Conference on Liquid Atomization and Spray Systems, September 6-8, Valencia, Spain*, 2017.

[53] Reid, R., Prausnitz, J., and Poling, B., *The Properties of Gases and Liquids*, McGraw-Hill, 1987.

[54] Ricou, F. P. and Spalding, D. B., Measurements of entrainment by axisymmetrical turbulent jets, *Journal of Fluid Mechanics*, vol. **11**, no. 1, p. 21–32, 1961.

[55] Robert, A., Martinez, L., Tillou, J., and Richard, S., Eulerian – Eulerian Large Eddy Simulations Applied to Non-Reactive Transient Diesel Sprays, *Oil & Gas Science and Technology – Revue d'IFP Energies nouvelles*, vol. **69**, no. 1, pp. 141–154, 2014.
URL `http://ogst.ifpenergiesnouvelles.fr/10.2516/ogst/2013140`

[56] Schmidt, D., Gopalakrishnan, S., and Jasak, H., Multi-dimensional simulation of thermal non-equilibrium channel flow, *International Journal of Multiphase Flow*, vol. **36**, no. 4, pp. 284 – 292, 2010.
URL `http://www.sciencedirect.com/science/article/pii/S030193220900192X`

[57] Shin, D. H., Sandberg, R. D., and Richardson, E. S., Self-similarity of fluid residence time statistics in a turbulent round jet, *Journal of Fluid Mechanics*, vol. **823**, pp. 1–25, 2017.

[58] Shinjo, J. and Umemura, A., Simulation of liquid jet primary breakup: Dynamics of ligament and droplet formation, *International Journal of Multiphase Flow*, vol. **36**, no. 7, pp. 513–532, 2010.

[59] Siebers, D., Liquid-phase fuel penetration in diesel sprays, *Trans. SAE*, vol. **107**, pp. 1205–1227, 1998.

[60] Siebers, D., Scaling liquid-phase fuel penetration in diesel sprays based on mixing-limited vaporization, *Trans. SAE*, vol. **108**, pp. 703–728, 1999.

[61] Siebers, D. L., 2008. Recent developments on diesel fuel jets under quiescent conditions, *Flow and combustion in reciprocating engines*. Arcoumanis, C. and Kamimoto, T. (Eds.). Springer-Verlag, Berlin, pp. 257–308.

[62] Taub, G. N., Lee, H., Balachandar, S., and Sherif, S. A., A direct numerical simulation study of higher order statistics in a turbulent round jet, *Physics of Fluids*, vol. **25**, no. 11, p. 115102, 2013.
URL `http://aip.scitation.org/doi/10.1063/1.4829045`

[63] Trask, N., Schmidt, D., Lightfoot, M., and Danczyk, S., Compressible modeling of the internal flow in a gas-centered swirl-coaxial fuel injector, *Journal of Propulsion and Power*, vol. **28(4)**, pp. 685–693, 2012.

[64] Vallet, A. and Borghi, R., Modélisation Eulerienne de l'atomisation d'un jet liquide, *C.R. Acad. Sci, Paris*, vol. **327**, pp. 1015–1020, 1999.

[65] Vallet, A., Burluka, A., and Borghi, R., Development of a Eulerian model for the "atomization" of a liquid jet, *Atomization and Sprays*, vol. **11**, pp. 619–642, 2001.

[66] Wehrfritz, A., Kaario, O., Vuorinen, V., and Somers, B., Large Eddy Simulation of n-dodecane spray flames using Flamelet Generated Manifolds, *Combustion and Flame*, vol. **167**, pp. 113–131, 2016.
URL `https://www.sciencedirect.com/science/article/pii/S0010218016000754?via%3Dihub`

[67] Weller, H., Tabor, G., Jasak, H., and Fureby, C., A tensorial approach to computational continuum mechanics using object-oriented techniques, *Computers in Physics*, vol. **12**, pp. 620–631, 1998.

[68] Xue, Q., Battistoni, M., Powell, C., Longman, D., Quan, S., Pomraning, E., Senecal, P., Schmidt, D., and Som, S., An eulerian CFD model and x-ray radiography for coupled nozzle flow and spray in internal combustion engines, *International Journal of Multiphase Flow*, vol. **70**, pp. 77 – 88, 2015.

[69] Xue, Q., Som, S., Senecal, P. K., and Pomraning, E., Large eddy simulation of fuel-spray under non-reacting ic engine conditions, *Atomization and Sprays*, vol. **23**, no. 10, pp. 925–955, 2013.